CHINESE OPTICS LETTERS

Vol. 21, No. 12 | December 2023

Simultaneous determination of polarization states and mode coefficients of fiber LP modes with four-channel off-axis holography

Zhigang Han (韩志刚)[1,2*], Junbo Li (李俊博)[1,2], Siliang Liu (刘斯靓)[1,2], Fangxin Li (李方欣)[1,2], Zhenying Yang (杨振营)[1,2], Qi Wang (王 琦)[1,2], Jiuduo Rui (芮九多)[1,2], Hua Shen (沈 华)[1,2], and Rihong Zhu (朱日宏)[1,2]

[1] School of Electronic Engineering and Optoelectronic Technology, Nanjing University of Science and Technology, Nanjing 210094, China

[2] MIIT Key Laboratory of Advanced Solid Laser, Nanjing University of Science and Technology, Nanjing 210094, China

*Corresponding author: hanzhigang@njust.edu.cn

Received May 4, 2023 | Accepted July 27, 2023 | Posted Online December 8, 2023

Four-channel off-axis holography is proposed to simultaneously understand the polarization states and the mode coefficients of linearly polarized (LP) modes in few-mode fiber. Far-field off-axis holograms in the four polarization directions of the fiber laser were acquired at the same moment through a four-channel holographic device. The weights, the relative phase differences, and the polarization parameters of the vector fiber laser mode can be solved simultaneously. The simulated and experimental mode analysis of the laser output by 1060-XP fiber with 6 LP modes at 632.8 nm is conducted, which shows that the similarity of the total intensity distribution of the laser before and after mode analysis is above 0.97. The mode polarization states, the mode weights, and the relative phase differences of the few-mode laser can be determined simultaneously in a single shot by four-channel off-axis holography.

Keywords: vectorial fiber laser; few-mode fiber; off-axis holography; mode decomposition.

DOI: 10.3788/COL202321.120601

1. Introduction

Recently, the development of few-mode fiber (FMF) has attracted much attention in frontier technologies[1–4]. For example, in telecommunications, spatial mode division multiplexing (MDM) technology based on FMFs is one of the best solutions to break the limit of communication capacity of single-mode fibers[1,2]. In high-power lasers, FMFs with larger mode field area can effectively improve the power thresholds of nonlinear effects[3,4]. For these applications, the mode coefficients of the eigenmodes, including mode weights and phase differences, are important parameters to characterize the mode field of few-mode lasers, which is the superposition of the products of the complex amplitudes and the corresponding mode coefficients of the eigenmodes.

So far, a variety of mode decomposition (MD) techniques that calculate the mode coefficients have been proposed, such as the spatial spectroscopy method[5–7], correlation analysis method[8–10], numerical analysis method[11–14], digital holography method[15,16], and the matrix analysis method[17]. Both mode weights and phase differences can be determined simultaneously using these methods. However, the few-mode lasers under test usually need to pass through a polarization generator before the lasers are analyzed by the MD setups, so the above methods can only determine the mode coefficients under a single polarization direction.

Some researchers studied the determinations of the polarization states of the eigenmodes in FMFs. Flamm *et al.*[18] achieved Stokes vector measurement of different polarization modes in a six-mode fiber by adding a polarizer and a quarter-wave plate before the MD optical path based on the optical correlation filter method (CFM). Andrmahr *et al.*[19] adopted a similar method to study the polarization evolution of each mode during the increase of output power of fiber lasers. The polarization parameters of each mode were measured separately by introducing the polarizing elements into the MD system based on the annular cavity. However, these methods require multiple independent mode analysis, which rotates the analyzer or quarter-wave plate repeatedly. It is time-consuming and only suitable for the measurements of static beams.

In this paper, we propose a four-channel off-axis holographic method to understand both the mode coefficients and the polarization states of the linearly polarized (LP) mode in FMF. The light under test interferes with the reference light on the target of the polarization camera with four polarization channels, forming four off-axis holograms with different

polarization directions simultaneously. We can obtain the near-field complex amplitudes in each polarization direction by demodulating these single-shot far-field off-axis holograms[20] and transmitting them virtually. The mode weights, the relative phase differences, and the mode polarization states of the few-mode laser can be obtained based on the near-field complex amplitudes.

2. Theory

In FMF, the mode field can be characterized by a linear superposition of LP modes[18]. As shown in Fig. 1, each LP mode includes more than one spatial degenerate mode in the red frame and each spatial degenerate mode has two polarization degenerate modes in the blue frame. The two polarization degenerate modes with orthogonal polarization directions can be regarded as one mode in the same spatial distribution with a specific polarization state. Thus, the vector field of the laser can be determined by the polarized superposition of the LP modes,

$$\overrightarrow{E(x,y)} = a \cdot \sum_{m=1}^{M} (\rho_m \cdot e^{i\vartheta_m}) \cdot E_m(x,y) \cdot \overrightarrow{P_m}, \tag{1}$$

where the arrow $\vec{\cdot}$ represents the vector, M is the total number of modes supported by the fiber, ρ_m is the mode weight of the mth-order mode, and ρ_m^2 is proportional to the power ratio of the mth-order mode. ϑ_m is the phase difference of the mth-order mode and the base mode; $\overrightarrow{P_m}$ represents the polarization of the mth-order mode; $E_m(x,y)$ is the complex amplitude distribution of the LP eigen modes, and a is the amplitude coefficient.

According to the Jones vector, the polarization state $\overrightarrow{P_m}$ of the mth-order mode can be expressed as

$$\overrightarrow{P_m} = \frac{1}{\sqrt{A_m^2 + B_m^2}} \begin{bmatrix} A_m \\ B_m e^{i\varphi_m} \end{bmatrix}, \tag{2}$$

where A_m and B_m are both positive real numbers, which, respectively, indicate the intensity relationship in the orthogonal polarization directions. $\varphi_m \in [-\frac{\pi}{2}, \frac{\pi}{2}]$ represents the phase difference of the vectorial modes in orthogonal directions.

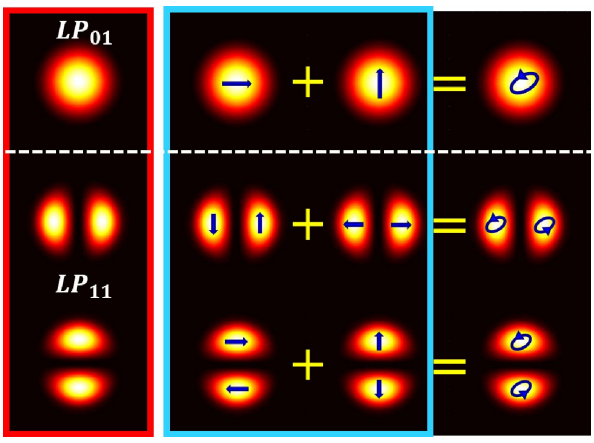

Fig. 1. Superposition of polarization-degenerate modes (blue frame) in the same spatial distribution.

As shown in Fig. 2, we present a four-channel off-axis holographic technique for mode decomposition of vectorial fiber laser. The light source is divided into two branches by the 1×2 fiber coupler (FC). One branch passes through the variable optical attenuator (VOA) and the FMF modulated by a polarization controller (PC), forming the light under test. The other passes through the VOA and the single-mode fiber modulated by a PC, forming the point-diffraction reference light. After passing the free-space nonpolarizing cube beam splitters (NPBSs), the light under test interferes with the reference light at the polarization camera, which is composed of the microlenses, the pixelated polarizers, and the surface detector. There are four orientations of the pixelated polarizers, which are 0°, 45°, 90°, and 135°[21]. Four off-axis holograms are collected by the polarization camera simultaneously. The off-axis amounts of the holograms can be adjusted by the relative radial position of the reference fiber and the fiber under test. The off-axis hologram of each polarization orientation can be expressed as

$$I_{\mathrm{int}_p}(x,y) = A_p(x,y) + C_p(x,y)\cos[\varphi_p(x,y) + w_1 \cdot x + w_2 \cdot y], \tag{3}$$

where $A_p(x,y) = I_p(x,y) + \check{I}_p(x,y)$ is the background of the hologram. $C_p(x,y) = 2\sqrt{I_p(x,y) \cdot \check{I}_p(x,y)}$ is the contrast of the hologram. $\check{I}_p(x,y)$ and $I_p(x,y)$ are the intensity distribution of the reference and the light under test. $\varphi_p(x,y)$ is the phase delay of the light under test regarding the reference light. w_1 and w_2 are the carrier frequency coefficients in the x and y axis.

The background intensity of the hologram $I_{p\_\mathrm{FT}}(x,y)$ and phase difference distribution $\varphi_{p\_\mathrm{FT}}(x,y)$ between the reference light and the light under test can be obtained by making a Fourier analysis to the off-axis holograms. Thus, the intensity of the light under test can be expressed as

$$I_{p\_\mathrm{in}}(x,y) = I_{p\_\mathrm{FT}}(x,y) - \check{I}_p(x,y), \tag{4}$$

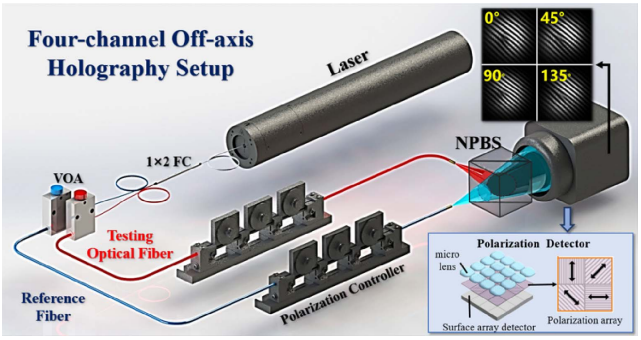

Fig. 2. Setup with four-channel off-axis holography.

where $\check{I}_p(x,y)$ is the reference light intensity of the pth polarization orientation.

Considering that the reference light is the LP_{01} mode, it has the same curvature radius of the spherical waves as the light under test at the target of the polarization camera, and the phase $\varphi_{p\_FFT}(x,y)$ after eliminating the phase tilt can be directly considered as the plane wave phase output by the light under test through the collimation lens. Further, the complex amplitude $E_{p_{in}}(x,y)$ of the light under test at the target of the polarization camera can be defined as

$$E_{p_{in}}(x,y)=\sqrt{I_{p\_in}(x,y)}\exp[i\varphi_{p\_FFT}(x,y)]. \tag{5}$$

Due to the large difference between the size of holograms and the fiber core, the mode field of the fiber end surface reconstructed by the complex amplitude obtained in Eq. (5) is low-resolution. To solve this problem, the virtual transmission method based on 4F system is used to obtain the enlarged complex amplitude distribution $E_p(x,y)$ at the conjugated position of the end surface of the fiber core in each channel[16]. The coefficient c_{mp} of the mth-order mode on the pth channel can be calculated by the cross-correlation degree[22],

$$c_{mp}=\frac{\iint E_p(x,y)E_m(x,y)\mathrm{d}x\mathrm{d}y}{\sqrt{\left(\iint |E_p(x,y)|^2\mathrm{d}x\mathrm{d}y\right)\iint |E_m(x,y)|^2\mathrm{d}x\mathrm{d}y}}, \tag{6}$$

where $E_m(x,y)$ is the ideal eigenmode distribution of the mth-order mode. The mode weights and the relative phase differences on the pth channel can be expressed as

$$\theta_{mp}=\arctan\left[\frac{\mathrm{Im}(c_{mp})}{\mathrm{Re}(c_{mp})}\right], \tag{7}$$

$$\mathrm{rho}_{mp}=\mathrm{Re}(c_{mp})^2+\mathrm{Im}(c_{mp})^2, \tag{8}$$

where rho_{mp} satisfies the relationship: $\sum|c_{mp}|^2=\sum\mathrm{rho}_{mp}=1$.

Through the mode analysis, the intermodal relationship on each channel can be obtained. According to the generalized polarization theory[23], to determine the polarization parameters of LP modes, the above intermodal relationship needs to be converted into the light intensity relationship of each mode in different polarization directions ulteriorly.

The complex amplitude $E_{Rmp}(x,y)$ of LP modes in each channel can be expressed as

$$E_{Rmp}(x,y)=\sqrt{K_p}\cdot\sqrt{\mathrm{rho}_{mp}}\cdot e^{i\theta_{mp}}\cdot E_m(x,y), \tag{9}$$

where $K_p=\iint I_p(x,y)\mathrm{d}x\mathrm{d}y/\iint I\_R_p(x,y)\mathrm{d}x\mathrm{d}y$ is the intensity ratio of the pth channel, $I_p(x,y)$ and $I\_R_p(x,y)$ refer to the actual intensity distribution and the reconstruction by the normalized mode decomposition coefficients on the pth channel.

The Stokes parameters express the state of polarization in matrix defined as[23]

$$S(x,y)=\begin{bmatrix}S_0(x,y)\\S_1(x,y)\\S_2(x,y)\\S_3(x,y)\end{bmatrix}=\begin{bmatrix}I_{0^\circ}(x,y)+I_{90^\circ}(x,y)\\I_{0^\circ}(x,y)-I_{90^\circ}(x,y)\\I_{45^\circ}(x,y)-I_{135^\circ}(x,y)\\I_{\mathrm{Right}}(x,y)-I_{\mathrm{Left}}(x,y)\end{bmatrix}, \tag{10}$$

where the $I_{0^\circ}(x,y)$, $I_{45^\circ}(x,y)$, $I_{90^\circ}(x,y)$, and $I_{135^\circ}(x,y)$ are the intensities measured by pixels corresponding to polarizers oriented at 0°, 45°, 90°, and 135°, respectively, while $I_{\mathrm{Right}}(x,y)$ and $I_{\mathrm{Left}}(x,y)$ are intensities that represent the amount of right-handed and left-handed circularly polarized light.

If the LP modes are fully polarized, the Stokes parameters can be determined by the mode weight rho_{mp} and the intensity ratio K_p of the pth channel,

$$S_{0m}=I_{0^\circ}+I_{90^\circ}\propto \mathrm{rho}_{m1}\cdot K_1+\mathrm{rho}_{m3}\cdot K_3, \tag{11a}$$

$$S_{1m}=I_{0^\circ}-I_{90^\circ}\propto \mathrm{rho}_{m1}\cdot K_1-\mathrm{rho}_{m3}\cdot K_3, \tag{11b}$$

$$S_{2m}=I_{45^\circ}-I_{135^\circ}\propto \mathrm{rho}_{m2}\cdot K_2-\mathrm{rho}_{m4}\cdot K_4, \tag{11c}$$

$$|S_{3m}|=\sqrt{S_{0m}^2-S_{1m}^2-S_{2m}^2}. \tag{11d}$$

It also can be represented by the parameters of the polarization vector $\overrightarrow{P_m}$ in Eq. (2)[23],

$$S_{0m}=A_m^2+B_m^2, \tag{12a}$$

$$S_{1m}=A_m^2-B_m^2, \tag{12b}$$

$$S_{2m}=2A_mB_m\cos(\varphi_m), \tag{12c}$$

$$S_{3m}=2A_mB_m\sin(\varphi_m). \tag{12d}$$

Each parameter of the polarization vector $\overrightarrow{P_m}$ of the mth-order mode can be expressed by the mode weight rho_{mp} and the intensity ratio K_p of each channel,

$$A_m=\sqrt{\frac{S_{0m}+S_{1m}}{2}}=\sqrt{\mathrm{rho}_{m1}\cdot K_1}, \tag{13a}$$

$$B_m=\sqrt{\frac{S_{0m}-S_{1m}}{2}}=\sqrt{\mathrm{rho}_{m3}\cdot K_3}, \tag{13b}$$

$$\begin{aligned}|\varphi_m|&=\arccos\left(\frac{S_{2m}}{2A_mB_m}\right)\\&=\arccos\left(\frac{\mathrm{rho}_{m2}\cdot K_2-\mathrm{rho}_{m4}\cdot K_4}{2\sqrt{\mathrm{rho}_{m1}\cdot K_1\cdot\mathrm{rho}_{m3}\cdot K_3}}\right)\in[0,\pi).\end{aligned} \tag{13c}$$

Comparing the expression of Eq. (9) with Eq. (1) on the 0° channel, ρ_m and ϑ_m in the vectorial laser can be expressed as

$$\vartheta_m=\theta_{m1}, \tag{14a}$$

$$\rho_m \propto \sqrt{\mathrm{rho}_{m1} \cdot K_1 + \mathrm{rho}_{m3} \cdot K_3}, \tag{14b}$$

where ρ_m satisfies the relationship: $\sum \rho_m^2 = 1$.

It should be noted that the sign of φ_m cannot be determined by Eq. (13c). In other words, the polarization rotation direction of the modes cannot be calculated directly. In order to solve this problem, we exhaust the different polarization rotations by varying the sign of φ_m, and joint Eqs. (13) and (14) into Eq. (1) to obtain the superposition of LP modes with different rotations. Comparing the similarity of the above results and the incoherent superposition of the mode field in each channel after the demodulation of off-axis holograms, the sign with the highest similarity is the final result.

In summary, the polarization states and the mode coefficients of the LP modes can be calculated by four-channel off-axis holograms. Figure 3 summarizes the calculation flow. First, we obtain the complex amplitude in the four channels at the camera target by solving the off-axis hologram based on the frequency carrier method[24,25]. Second, the mode fields of the fiber end in the conjugated position of each channel are established by a virtual 4F system. Third, the mode weights and the relative phase differences of the fiber laser in each channel are calculated by complex amplitude projection[26]. Finally, the mode weights, the relative phase differences, and the mode polarization parameters of the vectorial LP modes can be obtained with polarization mode analysis.

3. Simulation

A simulation model is developed to verify the method. The fiber under test (core diameter, 5.8 μm; NA, 0.14) is consistent with the 1060-XP fiber (Nufern), which contains six LP modes at the wavelength of 632.8 nm. The reference fiber (fiber core diameter, 3.5 μm; NA, 0.13) is consistent with the 630HP fiber (Nufern), which is a single-mode fiber at the wavelength of 632.8 nm. Figure 4(a) shows the mode weights and the relative phase differences of the test laser. The mode weights of LP_{01}, LP_{11o}, LP_{21e}, and LP_{21o} are set to 0.2; others are set to 0.1. Figure 4(b) is the representation of each mode polarization on the Poincaré sphere. The six dots on the Poincaré sphere corresponding to each LP mode are connected in the order of LP_{01}, LP_{11e}, LP_{11o}, LP_{02}, LP_{21e}, and LP_{21o}. Figure 4(c) shows the total intensity distribution of the vectorial beam with the parameters above, which is the incoherent superposition of the projected complex amplitudes in orthogonal polarization directions of $\overrightarrow{E(x,y)}$. As is shown, the total intensity at the end of the test fiber is concentrated in a circle with a radius of 5.8 μm. Figure 4(d) shows the total intensity distribution of the circularly-polarized reference light, which is mainly Gaussian, distributed in a circle with a radius of 3.5 μm.

Figure 5 shows the simulated off-axis hologram formed in the 0° polarization channel of the polarization camera and its demodulation results. In the simulation, the transmission distance from the fiber end to the camera target is set to 0.1 mm, in order to minimize the spectral undersampling problem[27] during angular spectrum transmission. The hologram shown in Fig. 5(a) is mainly distributed in a square with a length of 40 μm. There are six fringes in a circle with a diameter of 5 μm. Figure 5(b) shows the spectral information. Figure 5(c) shows the intensity distribution of the test light in the 0° polarization channel, obtained by performing the inverse Fourier transform of the 0th-order frequency component in Fig. 5(b)

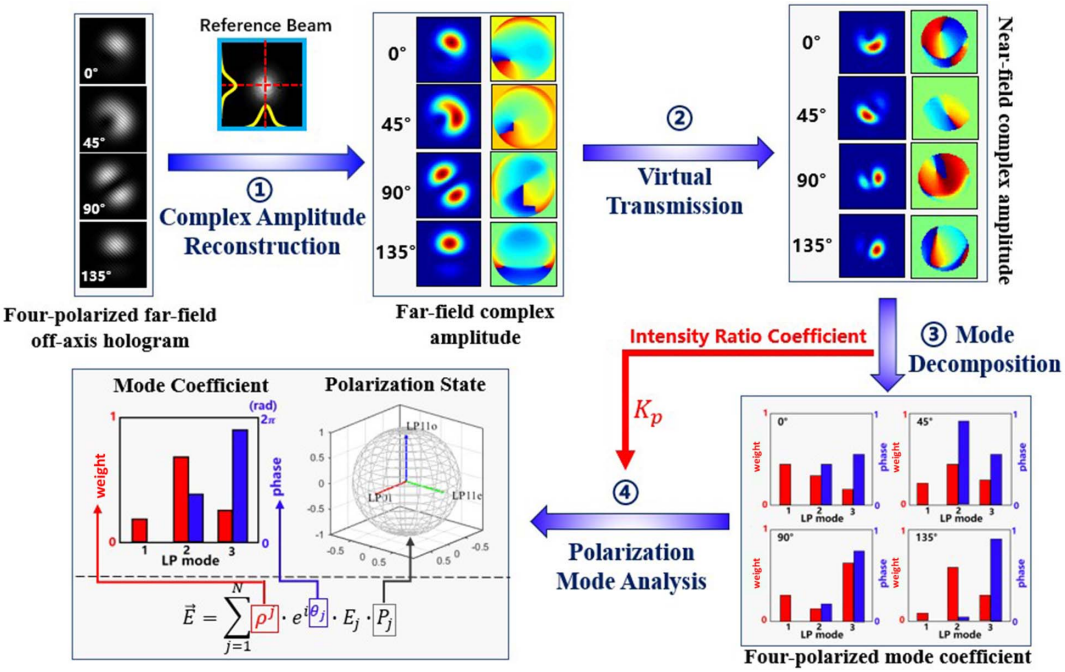

Fig. 3. Simulation process.

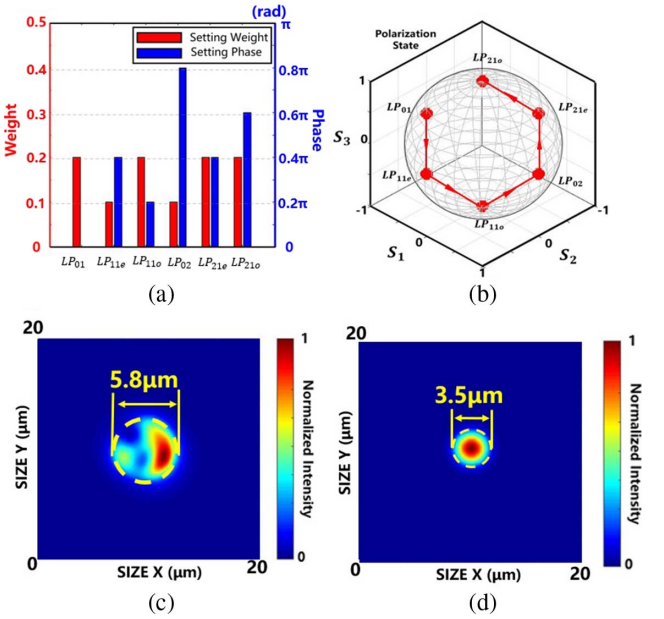

Fig. 4. Parameter of vectorial laser and light intensity distribution. (a) Mode coefficient set in the simulation; (b) set values of the mode polarization states; (c) intensity of the test light; (d) intensity of the reference light.

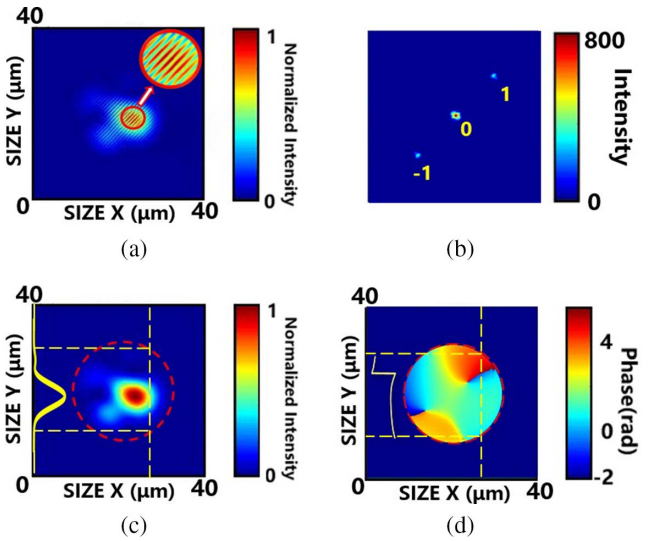

Fig. 5. Off-axis hologram of 0° channel and its demodulation results. (a) Off-axis hologram; (b) local spectral distribution; (c) demodulation results of the light intensity; (d) demodulation results of the phase distribution.

and excluding the precollected reference light. The phase distribution in the same channel is shown in Fig. 5(d), which is obtained by performing the inverse Fourier transform of the −1st-order frequency component in Fig. 5(b).

Figure 6(a) shows the calculated light intensity distribution of the fiber end in the 0° polarization channel using the virtual transmission method[16]. Light intensity varies in each polarization channel due to the different polarization states of LP modes. Figure 6(b) shows the MD results on the 0° channel, including the mode weights and the relative phase differences. Figure 6(c) shows the reconstruction by MD on the 0° polarization channel. The light intensity similarity before and after MD reconstruction is 0.9996. The similarities on other channels (45°, 90°, and 135°) are 0.9987, 0.9981, and 0.9993 respectively. All of them remained above 0.99, which can verify the feasibility of the MD.

Figures 7(a) and 7(b) represent the mode weights and the relative phase differences of the vectorial LP modes determined by Eqs. (14a) and (14b). The solid and striped bar charts represent the set values and the calculated results, which are consistent with each other. Figure 7(c) represents the set polarization states (red) and the calculated ones (blue) of each mode on the Poincaré sphere. The total intensity distribution reconstructed by the above mode coefficients and polarization states of LP modes is shown in Fig. 7(d). The similarity between the distribution in the figure and that in Fig. 4(c) is 0.9883, proving that this new method can simultaneously understand the polarization states and the mode coefficients of LP modes.

4. Experimental Setup

Figure 8 shows the experimental setup based on the four-channel off-axis holography. A He–Ne laser ($\lambda = 632.8$ nm, HRS015B, Thorlabs) is used as the light source. The light source is coupled into a 1×2 fiber optic splitter (MCFBT, MC Light, China) with a coupler (PAF2-A4C, Thorlabs). Both arms of the splitter are connected in turn with a VOA (MCVOA-630, MC Light, China) and a three-paddle PC (FPC030, Thorlabs), forming the reference light and the test light, respectively. 1060-XP fiber (core diameter, 5.8 μm; NA, 0.14; length, 2 m, Nufern) is used as the test fiber, which contains six LP modes at the wavelength of 632.8 nm. The single-mode fiber (Nufern, 630-HP) is used as the reference fiber. In Fig. 8, the area circled by the solid yellow line is the four-channel off-axis holographic system, which is ultracompact within 50 mm × 30 mm × 30 mm. The holograms taken by the polarization camera (PHX050S, Lucid) are analyzed by personal computer (Lenovo Y7000P, CPU i7-10875 H, RAM 16G).

5. Results

Figures 9(a)-9(d) show the intensity distribution of the reference light on each channel of the polarization camera. The reference light is generated by the single-mode fiber with the polarization states controlled by the three-paddle PC. As is shown, the intensity on each channel conforms to the Gaussian distribution. Figure 9(e) shows the degree of linear polarization (DOLP), which is calculated by the method described in the literature[21]. Since the DOLP values in the figure are all close to 0, the reference light is circularly polarized.

Figures 10(a)–10(d) show the four-channel holograms taken by the polarization camera in a single shot. The exposure time of the camera is 33 μs. Intensity and phase distributions of the test light, which is demodulated by holograms, are shown in Figs. 10(e)–10(h) and 10(i)–10(l). The tilt aberrations of the

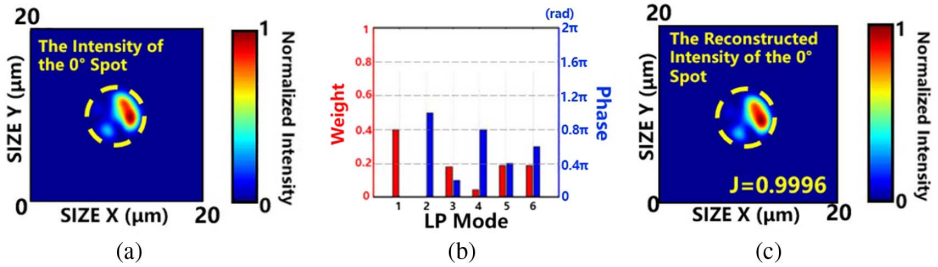

Fig. 6. Light intensity distribution in the conjugated position of the fiber end and its MD reconstruction in the 0° channel. (a) Light intensity after virtual transmission; (b) MD coefficients; (c) reconstruction by MD.

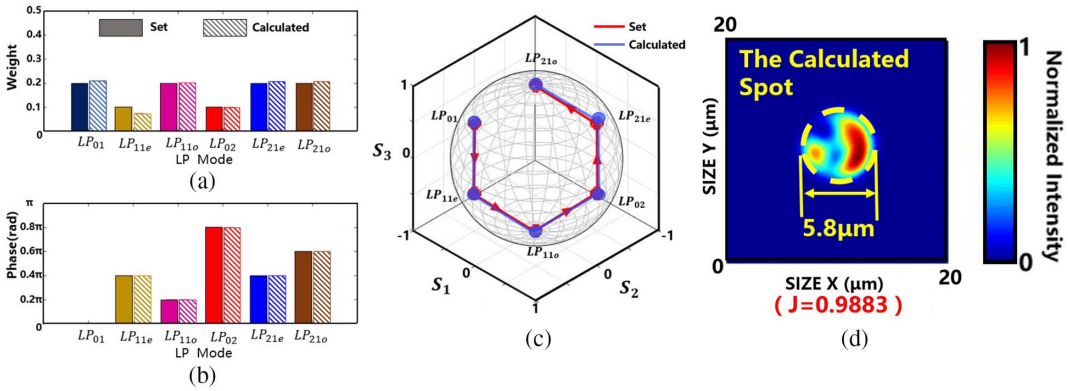

Fig. 7. Simulation results of mode analysis. (a) Mode weights; (b) relative phase differences; (c) mode polarization states; (d) reconstruction after mode analysis.

demodulated phase distributions are eliminated. There are obvious phase steps in the weak intensity positions, which shows that the tilt aberrations are effectively eliminated. Since the reference light is fixed, dynamic demodulations of the holograms can be achieved when a set of reference light intensity is pre-acquired.

Figures 11(a) and 11(b) show the normalized total intensity distributions, which is the incoherent superposition of the projected complex amplitudes in the orthogonal polarization directions of $\overrightarrow{E(x,y)}$ before and after mode analysis. The similarity between them is up to 0.9933. Figure 11(c) shows the mode weights (red) and relative phase differences (blue). The LP_{11e} and LP_{11o} are the main components in this mode field. Figure 11(d) shows the polarization states of modes calculated by mode analysis on a Poincaré sphere. LP_{11o}, LP_{21e}, and LP_{21o} are nearly linear polarization. LP_{01}, LP_{02}, and LP_{11o} are elliptically polarized. Through disturbing the test fiber by the PC, we take 30 groups of holograms for mode analysis. The acquisition of each group of holograms can be achieved by a single exposure of the polarization camera, so the acquisition time is extremely fast. However, the post-acquisition analysis can be on the order of several minutes, depending on the data size of the images. The top and bottom spots of Fig. 12 are the total intensity reconstructed before and after mode analysis, respectively. The 30 sets of total intensity similarities between them are all above 0.97, demonstrating this method is robust.

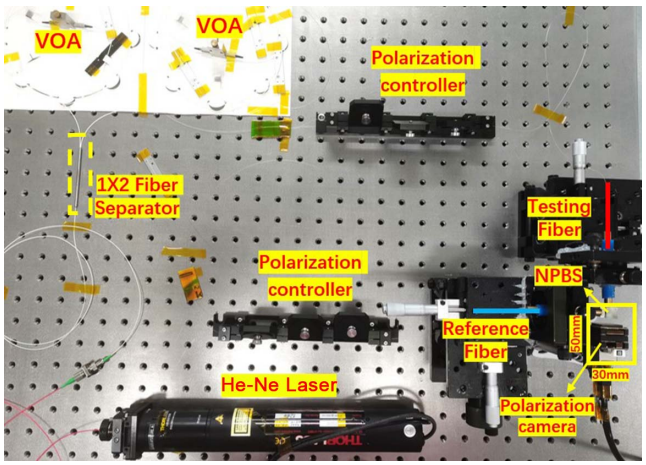

Fig. 8. Experimental setup.

6. Discussions

The polarization state of the reference light influences the demodulation accuracy of the testing light complex amplitude and the mode analysis results by affecting the contrast of the hologram in each channel. Based on the laser parameters set in the simulation, Figs. 13(a) and 13(b) show the mode analysis results when the reference light is on elliptic and linear polarization states. The total intensity similarities before and after mode analysis are 0.9939 and 0.9652 when the reference light is elliptically and linearly polarized, respectively. The similarity of the total intensity before and after mode analysis in Fig. 13(a)

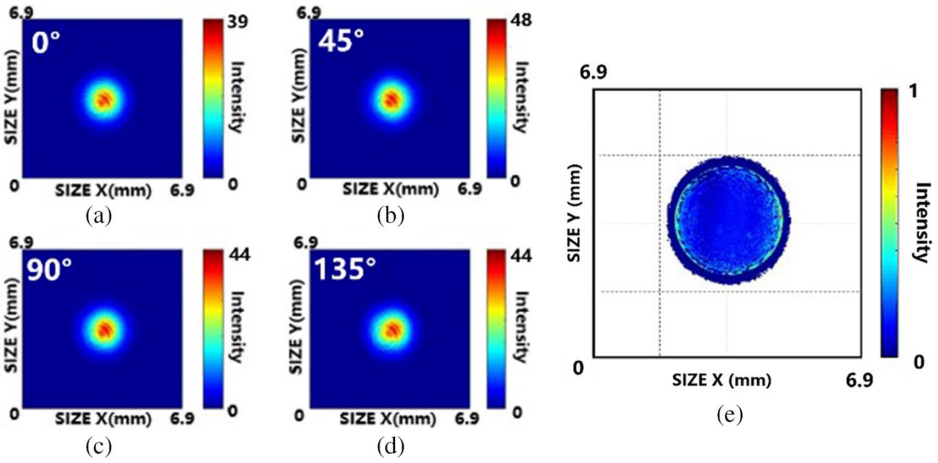

Fig. 9. Reference light intensity on each channel and its DOLP distribution. (a)–(d) Intensity of the reference light on different channels; (e) DOLP distribution of the reference light.

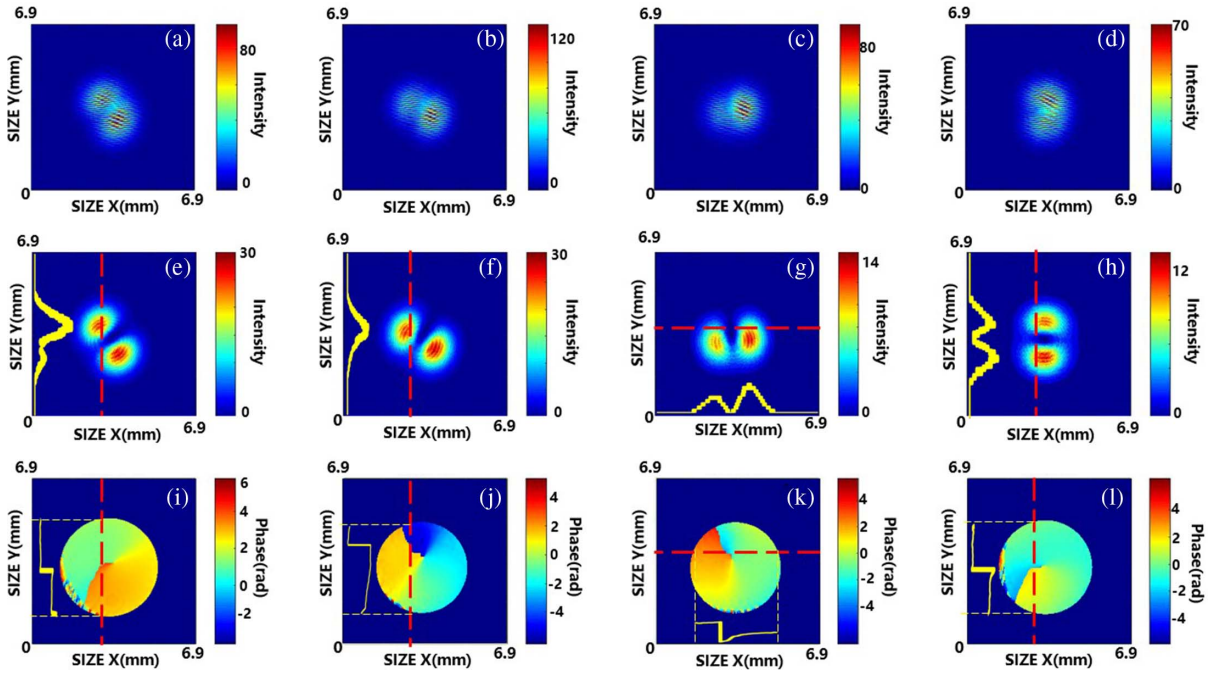

Fig. 10. Holograms in each channel and its demodulation results. (a)–(d) Holograms; (e)–(h) demodulation results of the intensity; (i)–(l) demodulation results of the phase.

is basically the same as that in Fig. 7(d), while the similarity in Fig. 13(b) differs from that in Fig. 7(d). Figure 13(c) shows that the polarization states of different LP modes measured with the elliptically polarized reference light are consistent with the set values, while the results measured with the linearly polarized light are different. This phenomenon can be attributed to the fact that the contrast of the off-axis hologram is close to 0 on the channel whose polarization axis is orthogonal to that of the linearly polarized reference light. Thus, the linearly polarized reference light cannot be used for the mode analysis with the four-channel off-axis holography.

Figure 14 shows the effects of the remaining tilt and defocus aberrations in the demodulated phase distribution in Fig. 5(d) on mode analysis. The results show that when the tilt aberration (red line) exceeds 1λ ($\lambda = 633$ nm), its similarity of the total intensity before and after mode analysis is lower than 0.96. As for the defocus aberration (blue line), the total intensity similarity before and after mode analysis is lower than 0.95. In the experiment, the stripes of the holograms should be kept as straight as possible to reduce the effects of the defocus aberration. At the same time, the tilt aberration should be eliminated in the demodulation process of the holograms according to the

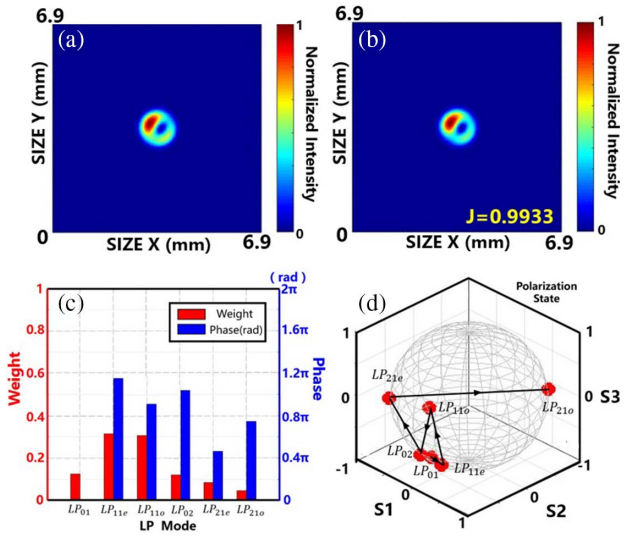

Fig. 11. Mode analysis results. (a) Reconstruction by MD; (b) reconstruction by mode analysis; (c) mode coefficients; (d) polarization states.

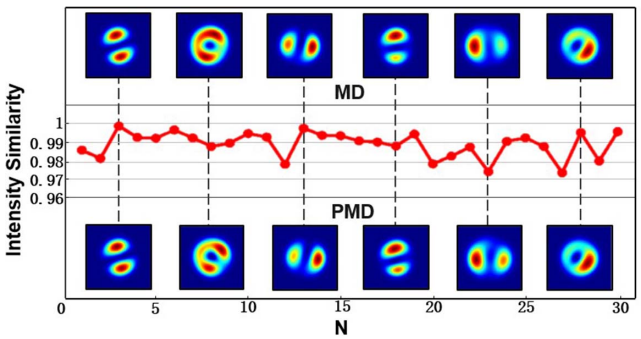

Fig. 12. Similarities of different MD calculations.

step phase characteristics of the mode field to obtain more accurate mode analysis results.

7. Conclusion

A four-channel off-axis holography is proposed to simultaneously understand the polarization states and the mode coefficients of LP modes in FMF. Far-field off-axis holograms in the four polarization directions of the few-mode laser are acquired synchronously through a four-channel holographic device. Combined with the Fourier analysis of the holograms and the virtual transmission, the amplitude distributions on the fiber end in the four polarization channels are reconstructed with high precision and high resolution. By converting the intermodal relationship of each channel into the intensity relationship of each mode in the four channels, the weights, the relative phase differences, and the polarization parameters of the vectorial LP modes can be determined simultaneously. The combination of polarization camera and off-axis holographic technology enables single-shot mode analysis. The similarity of total intensity, which is the incoherent superposition of the projected complex amplitudes in the orthogonal polarization directions before and after mode analysis, is up to 0.9933 in experiment, demonstrating that the mode analysis is accurate. The method provides a technical solution for the determination of polarization states and mode coefficients of few-mode fiber and its devices, which is conducive to the design, manufacture, and development of fiber laser.

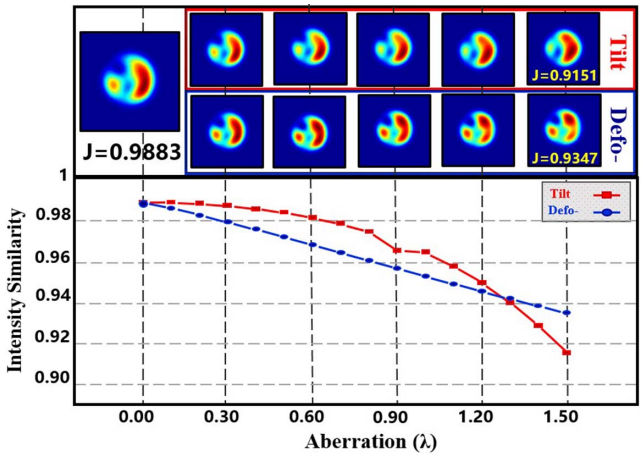

Fig. 14. Effects of the remaining tilt and defocus aberrations on mode analysis.

Acknowledgement

This work was supported by the National Natural Science Foundation of China (No. 61875087).

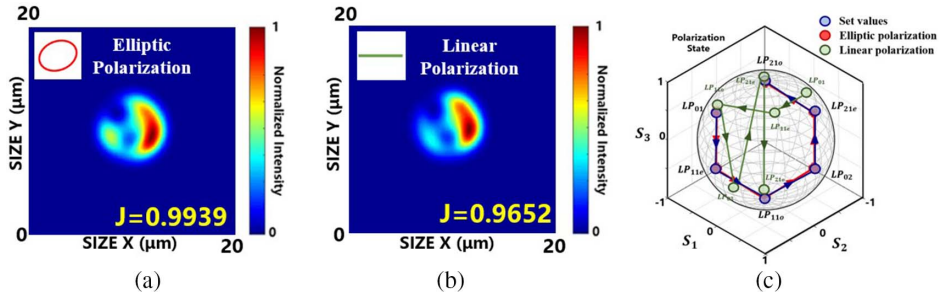

Fig. 13. Mode analysis results based on the reference light on different polarization states. (a) Elliptic polarization; (b) linear polarization; (c) polarization analysis results based on the reference light on different polarization states.

References

1. D. J. Richardson, J. M. Fini, and L. E. Nelson, "Space-division multiplexing in optical fibres," Nat. Photonics **7**, 354 (2013).
2. Z. He, X. Li, and M. Luo, "Independent component analysis based channel equalization for 6 × 6 MIMO-OFDM transmission over few-mode fiber," Opt. Express **24**, 9209 (2016).
3. J. Lv, C. Dai, and H. Li, "High-efficiency mode-locked fiber laser with a switchable oscillating transverse mode in an all few-mode fiber linear cavity," Opt. Express **30**, 1641 (2022).
4. M. Jiang, P. Zhou, H. Xiao, and P. F. Ma, "A high-power narrow-linewidth 1018 nm fiber laser based on a single-mode–few-mode–single-mode structure," High Power Laser Sci. Eng. **3**, E25 (2015).
5. J. W. Nicholson, A. D. Yablon, S. Ramachandran, and S. Ghalmi, "Spatially and spectrally resolved imaging of modal content in large-mode-area fibers," Opt. Express **16**, 7233 (2008).
6. H. J. Otto, F. Jansen, F. Stutzki, C. Jauregui, J. Limpert, and A. Tunnermann, "Improved modal reconstruction for spatially and spectrally resolved imaging (S^2)," J. Lightwave Technol. **31**, 1295 (2013).
7. Y. An, H. Yang, X. Chen, L. Huang, Z. Yan, Z. Pan, Z. Wang, Z. Jiang, and P. Zhou, "Seeing the strong suppression of higher order modes in single trench fiber using the S^2 technique," Opt. Lett. **48**, 61 (2023).
8. D. Benedicto, M. V. Collados, J. C. Martín, J. Atencia, O. Mendoza-Yero, and J. A. Vallés, "Contribution to the improvement of the correlation filter method for modal analysis with a spatial light modulator," Micromachines **13**, 2004 (2022).
9. J. Pinnell, I. Nape, B. Sephton, M. A. Cox, V. Rodríguez-Fajardo, and A. Forbes, "Modal analysis of structured light with spatial light modulators: a practical tutorial," J. Opt. Soc. Am. A **37**, C146 (2020).
10. M. D. Gervaziev, I. Zhdanov, D. S. Kharenko, V. A. Gonta, V. M. Volosi, E. V. Podivilov, S. A. Babin, and S. Wabnitz, "Mode decomposition of multimode optical fiber beams by phase-only spatial light modulator," Laser Phys. Lett. **18**, 015101 (2021).
11. Y. An, L. Huang, J. Li, J. Leng, L. Yang, and P. Zhou, "Learning to decompose the modes in few-mode fibers with deep convolutional neural network," Opt. Express **27**, 10127 (2019).
12. Q. Zhang, S. Rothe, N. Koukourakis, and J. Czarske, "Learning the matrix of few-mode fibers for high-fidelity spatial mode transmission," APL Photonics **7**, 066104 (2022).
13. Z. Tian, L. Pei, J. Wang, K. Hu, W. Xu, J. Zheng, J. Li, and T. Ning, "High-performance mode decomposition using physics- and data-driven deep learning," Opt. Express **30**, 39932 (2022).
14. Y. Liu, Q. Liu, J. Xiong, S. Zhao, M. Lyu, X. Pan, J. Zhang, and Z. He, "Complete modal decomposition of a few-mode fiber based on ptychography technology," Opt. Lett. **47**, 5813 (2022).
15. M. Lyu, Z. Lin, G. Li, and G. Situ, "Fast modal decomposition for optical fibers using digital holography," Sci. Rep. **7**, 6556 (2017).
16. J. Li, Z. Han, and R. Zhu, "Fast fiber mode decomposition with a lensless fiber-point-diffraction interferometer," Opt. Lett. **46**, 2501 (2021).
17. E. S. Manuylovich, V. V. Dvoyrin, and S. K. Turitsyn, "Fast mode decomposition in few-mode fibers," Nat. Commun. **11**, 5507 (2020).
18. D. Flamm, O. A. Schmidt, C. Schulze, J. Borchardt, T. Kaiser, S. Schröter, and M. Duparré, "Measuring the spatial polarization distribution of multimode beams emerging from passive step-index large-mode-area fibers," Opt. Lett. **35**, 3429 (2010).
19. N. Andermahr, T. Theeg, and C. Fallnich, "Novel approach for polarization-sensitive measurements of transverse modes in few-mode optical fibers," Appl. Phys. B **91**, 353 (2008).
20. G. Pariente, V. Gallet, A. Borot, O. Gobert, and F. Quéré, "Space-time characterization of ultra-intense femtosecond laser beams," Nat. Photonics **10**, 547 (2016).
21. D. Vorobiev, Z. Ninkov, and M. Gartley, "Polarization in a snap: imaging polarimetry with micropolarizer arrays," Proc. SPIE **9099**, 909904 (2014).
22. Y. S. Lee, K. S. Lim, M. K. A. Zaini, and H. Ahmad, "Mode splitting based on polarization manipulation in few-mode fiber," IEEE J. Quantum Electron. **54**, 6800306 (2018).
23. H. G. Berry, G. Gabrielse, and A. E. Livingston, "Measurement of the Stokes parameters of light," Appl. Opt. **16**, 3200 (1977).
24. M. Takeda, H. Ina, and S. Kobayashi, "Fourier-transform method of fringe-pattern analysis for computer-based topography and interferometry," J. Opt. Soc. Am. **72**, 156 (1982).
25. E. Zendejas-Hernández, G. Trujillo-Schiaffino, and M. Anguiano-Morales, "Spatial and temporal methods for fringe pattern analysis: a review," J. Opt. **52**, 888 (2023).
26. Y. Liu, Q. Liu, and J. Xiong, "Complete modal decomposition of a few-mode fiber based on ptychography technology," Opt. Lett. **47**, 5813 (2022).
27. W. Zhao, C. Wei, C. Yuan, C. Chang, J. Ma, and R. Zhu, "A flexible numerical calculation method of angular spectrum based on matrix product," Opt. Lett. **45**, 5937 (2020).